

# A quantum Monte Carlo algorithm to extract large-scale data of entanglement entropy and its derivative in high precision

Zhe Wang,<sup>1,2</sup> Zhiyan Wang,<sup>1,2</sup> Yi-Ming Ding,<sup>1,2</sup> Bin-Bin Mao,<sup>3</sup> and Zheng Yan<sup>1,2,\*</sup>

<sup>1</sup>*Department of Physics, School of Science and Research Center for Industries of the Future, Westlake University, Hangzhou 310030, China*

<sup>2</sup>*Institute of Natural Sciences, Westlake Institute for Advanced Study, Hangzhou 310024, China*

<sup>3</sup>*School of Foundational Education, University of Health and Rehabilitation Sciences, Qingdao 266000, China*  
(Dated: July 16, 2024)

We propose a quantum Monte Carlo (QMC) scheme able to extract large-scale data of entanglement entropy (EE) and its derivative with high precision and low technical barrier. It opens a way to numerically detect the novel phases and phase transitions by scanning EE in a wide parameter-region in two and higher dimensional systems. In other words, in the same order of computational time, the previous methods could only get one EE data point, but we can obtain thousands (even more) of times EE data points along a physical parameter path. We then show the feasibility of using EE and its derivative to find phase transition points and to probe novel phases.

*Introduction.-* With the rapid development of quantum information, its intersection with condensed matter physics has been attracting more and more attention in recent decades [1, 2]. One important topic is to probe the intrinsic physics of many-body systems using the entanglement entropy (EE) [3–6]. For instance, among its many intriguing features, it offers a direct connection to the conformal field theory (CFT) and a categorical description of the problem under consideration [7–26]. Using EE to identify novel phase and critical phenomena represents a cutting-edge area in the field of quantum many-body numerics. A particularly recent issue is the dispute at the deconfined quantum critical point (DQCP) [27–29]. The EE at the DQCP, e.g., in the JQ model [30, 31], exhibits totally different behaviours compared with that in normal criticality within the Landau-Ginzburg-Wilson paradigm [20, 32–36]. According to the prediction from the unitary CFT [37, 38], the EE with a cornered cutting at the criticality should obey the behaviours  $s = al - bnl + c$ , where  $s$  is the EE and  $l$  is the length of the entangled boundary, in which the coefficient  $b$  can not be negative. However, some recent QMC studies shows that  $b$  is negative. which seemingly suggests the DQCP in the JQ model is not a unitary CFT, probably instead of a weakly first order phase transition [22, 34, 35]. In contrast, another recent work indicates that the sign of  $b$  is dependent on the cutting form of the entangled region. For a tilted cutting,  $b$  is positive and consistent with the emergent SO(5) symmetry at the DQCP [33]. All in all, the relationship between entanglement entropy and condensed matter physics has been growing increasingly closer recently.

How to obtain high-precision EE via quantum Monte Carlo (QMC) [39–49] with less computation cost and low technical barrier is still a huge challenge in large-scale quantum many-body computation. Although many algorithms have been developed to extract the EE [50–59], some of which can also achieve high precision, the details of the algorithm becomes more and more complex. The

key point of extracting the Rényi ratio  $R_A^{(2)} = Z_A^{(2)}/Z^2$  (here we choose the Rényi order to be two without loss of generality) is to calculate the overlap of these two different space-time manifolds,  $Z_A^{(2)}$  and  $Z^2$ , as shown in Fig.1 (a) and (b), and then get the ratio directly [50, 54]. Once the ratio  $R_A^{(2)} \rightarrow 0$ , the calculation becomes extremely difficult. Due to the area law of EE, the  $R_A^{(2)} \propto e^{-al}$  decays to zero quickly in large systems, where  $l$  is the perimeter of the entangled region. To overcome this difficulty, in the early days, the incremental method of the entangled region was involved [50, 51]. Its key point is one by one adding the lattice site into the entangled region and product the ratio of the process to obtain the final ratio. The process can be written as  $R_A^{(2)} = Z_A^{(2)}/Z^2 = \prod_{i=0}^{N_A-1} Z_{A_{i+1}}^{(2)}/Z_{A_i}^{(2)}$ , where the  $i$  means the number of lattice sites of the entangled region, i.e.,  $Z_{A_0}^{(2)} = Z^2$  and  $Z_{A_{N_A}}^{(2)} = Z_A^{(2)}$ . Through calculating each intermediate-process ratio  $Z_{A_{i+1}}^{(2)}/Z_{A_i}^{(2)}$ , the high precision  $R_A^{(2)}$  could be extracted. The shortage of this method is the number of lattice site should be integer which means the splitting of the process must be finite, thus some ratios  $Z_{A_{i+1}}^{(2)}/Z_{A_i}^{(2)}$  may still be closed to zero even after splitting. We have to note that, the replica manifold are changing during the calculation due to the intermediate processes in this method. It makes the technical barrier of QMC higher.

To solve the finite splitting problem mentioned above, the continually incremental algorithm of QMC has been developed [22, 53, 57]. A virtual process described by a general function  $Z_A^2(\lambda)$  is involved, where  $Z_A^2(\lambda = 1) = Z_A^2$  and  $Z_A^2(\lambda = 0) = Z^2$ . The problem becomes to calculate the ratio  $Z_A^2(\lambda = 1)/Z_A^2(\lambda = 0)$  which is equal to  $\prod_{i=0}^{N_A-1} Z_A^2(\lambda_{i+1})/Z_A^2(\lambda_i)$ . Here the  $\lambda$  is continuous from 0 to 1, thus the interval  $[0, 1]$  can be divided in to any pieces according to the calculation requirement. However, not only the  $\lambda$  needs to be changed during the sampling of  $Z_A^2(\lambda)$ , but also the entangled region still has

to be varied under each fixed  $\lambda$ , which actually strongly takes huge computational cost and highly improves the technical requirements of the method. Moreover, due to the virtually non-physical intermediate-processes, the results of these intermediate processes  $Z_A^2(\lambda \neq 1, 0)$  can not be effectively used which leads a lot of wastes.

In this paper, we propose a simple method without changing the space-time manifold during simulation, and the intermediate-process values are physical and valuable. The high-precision EE and its derivative can be obtained in less cost and low-technical barrier from now on.

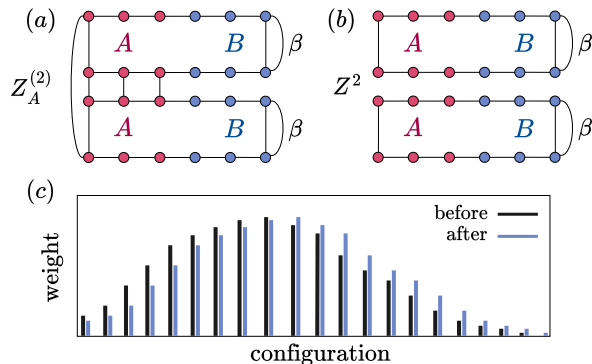


FIG. 1. A geometrical presentation of the partition function (a)  $Z_A^{(2)}$  and (b)  $Z^2$ . The entangling region  $A$  between replicas is glued together in the replica imaginary time direction and the environment region  $B$  for each replica is independent in the imaginary time direction. While the glued region is zero, it becomes back to  $Z^2$ . (c) Reweighting a same configuration: the sampled distribution (black, before reweighting) is used to reweight another distribution (blue, after reweighting), which is reasonable if these two distributions are close to each other as the importance sampling can be approximately kept.

**Method.-** The EE of a subsystem  $A$  coupled with an environment  $B$  is defined by the reduced density matrix (RDM). Specifically, The  $n$ th order Rényi entropy is defined as  $S^{(n)} = \frac{1}{1-n} \ln[\text{Tr}(\rho_A^n)] = \frac{1}{1-n} \ln R_A^{(n)}$ , where  $R_A^{(n)} = Z_A^{(n)}/Z^n$  and  $\rho_A = \text{Tr}_B \rho$ . From the above equations, we know that  $Z_A^{(n)} \propto \text{Tr}(\rho_A^n)$  while  $Z^n$  is the proportional factor.

The normalization factor  $Z^n$  sometimes is not important, for example, when we only concern the dynamical information of the entanglement Hamiltonian (e.g., entanglement spectrum) [26, 60–64]. In these cases, only the manifold of  $Z_A^{(n)}$  needs be simulated. However, when we consider the EE calculation, the factor becomes very important for the detailed value. In fact, the hardest difficulty of the calculation of EE comes from simulating the ratio  $R_A^{(n)} = Z_A^{(n)}/Z^n$ . That's the reason why the EE algorithms always have to change the simulating manifold between  $Z_A^{(n)}$  and  $Z^n$ .

Different from the traditional method calculating the ratio  $R_A^{(n)}$  directly, we start the calculation of  $Z_A^{(n)}$  and  $Z^n$  respectively. Here you may feel the sense why we do not need to change the manifold during the simulation. Given a certain distributional function, such as  $Z_A^{(n)}(J)$ , where  $J$  is a general parameter (e.g., temperature, the parameter of Hamiltonian, ...). For convenience, we define  $Z_A^{(1)} \equiv Z$  without losing generality. For two parameter points  $J'$  and  $J$ , the ratio can be simulated via QMC sampling:

$$\frac{Z_A^{(n)}(J')}{Z_A^{(n)}(J)} = \left\langle \frac{W(J')}{W(J)} \right\rangle_{Z_A^{(n)}(J)} \quad (1)$$

where the  $\langle \dots \rangle_{Z_A^{(n)}(J)}$  means the QMC samplings have been done under the manifold  $Z_A^{(n)}$  at parameter  $J$ .  $W(J')$  and  $W(J)$  denote the corresponding weights with different parameters  $J'$  and  $J$  for the same configuration sampled by QMC. It means that we simulate the system at parameter  $J$ , and then obtain a amount of configurations with weight  $W(J)$ , at the same time, we can calculate the related weight  $W(J')$  by treating the parameter as  $J'$  for the same configuration. The ratio of  $W(J')/W(J)$  can be calculated in each sampling to gain the final average as Eq.(1).

In principle, the ratio  $Z_A^{(n)}(J')/Z_A^{(n)}(J)$  of any  $J'$  and  $J$  can be solved in the way above. However, we still need to consider how to keep the importance sampling in our QMC simulation. Obviously, if the  $J'$  and  $J$  are close enough, the ratio is close to 1 and is easy for calculation. Otherwise, the ratio would be close to zero or infinite which can not be well-sampled by QMC. It can be easily understood in the reweighting frame as shown in Fig.1 (c), if we want to use a well-known distribution  $Z_A^{(n)}(J) = \sum W(J)$  to calculate another distribution  $Z_A^{(n)}(J') = \sum W(J')$  via resetting the weight of samplings, the weight before/after resetting of the same configuration should be close to each other. Then, it is still an importance sampling in this sense when the  $J'$  and  $J$  are close enough [65–67]. In fact, this spirit is also the key point of the incremental trick in previous EE algorithms. Therefore, we introduce the continuously incremental trick here to fix the problem:

$$\frac{Z_A^{(n)}(J')}{Z_A^{(n)}(J)} = \prod_{i=0}^{N-1} \frac{Z_A^{(n)}(J_{i+1})}{Z_A^{(n)}(J_i)} \quad (2)$$

where  $J_0 = J$  and  $J_N = J'$ , other  $J_i$  is between the two in turn. Thus the QMC can be kept in importance sampling through this reweight-annealing spirit [65, 67].

In this way, we are able to obtain any ratio  $Z_A^{(n)}(J')/Z_A^{(n)}(J)$  in realistic simulation. But it still can not give out the target solution of  $Z_A^{(n)}(J')/Z^n(J')$ . The antidote comes from some well-known point. Considering we have calculated the values of  $Z_A^{(n)}(J')/Z_A^{(n)}(J)$

and  $Z(J')/Z(J)$  from the method above, the problem  $Z_A^{(n)}(J')/Z^n(J') = ?$  will be solved if we know a reference point  $Z_A^{(n)}(J)/Z^n(J)$ . A simplest reference point is that the  $Z_A^{(n)}(J)/Z^n(J) = 1$  when the ground state is a product state  $|A\rangle \otimes |B\rangle$ . A product state is easy to be gained, for example, we can add an external field in a spin Hamiltonian to polarize all the spins, or a simplest way is decreasing the coupling between  $A$  and  $B$  to 0. Of course, other known reference points are also allowed, e.g., the status at infinite temperature or obtaining one known point through other numerical method. In fact, a lot of many-body Hamiltonians have a known ground state at the limit of parameter.

Now the whole scheme for extracting the Rényi EE is complete and realizable, it is not limited to the detailed QMC methods and many-body models. To further understand it and test its performance, we will show a  $J_1 - J_2$  spin model [68, 69] via using the stochastic series expansion (SSE) QMC [39–43, 70] as the example in the followings.

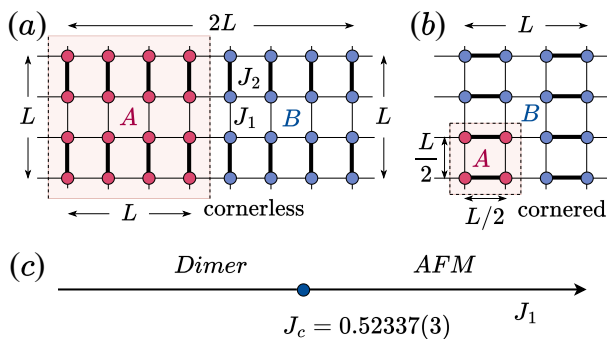


FIG. 2. Square lattice  $J_1$ - $J_2$  AFM Heisenberg model. The strong bonds  $J_2 > 0$  are indicated by thick lines. The weak bonds  $J_1 > 0$  are indicated by thin lines. (a) The entanglement region  $A$  is considered as a  $L \times L$  cylinder on the  $2L \times L$  torus with smooth boundaries and with the length of the entangling region  $l = 2L$ . (b) The entanglement region  $A$  is chosen to be a  $\frac{L}{2} \times \frac{L}{2}$  square with four corners and boundary length is  $l = 2L$ . (c) The diagram of the model setting strong bonds  $J_2 = 1$  in which quantum critical point (QCP) is  $J_1 = J_c = 0.52337(3)$  [68].

**$J_1 - J_2$  model.**- We simulate a 2D spin-1/2 antiferromagnetic (AFM) Heisenberg  $J_1 - J_2$  model as an example to obtain its EE. The Hamiltonian is

$$H = J_1 \sum_{\langle ij \rangle} S_i S_j + J_2 \sum_{\langle ij \rangle} S_i S_j \quad (3)$$

where  $\langle ij \rangle$  means the nearest neighbor bond, and  $J_1$  and  $J_2$  are the coupling strengths of thin and thick bonds as shown in Fig.2 and its ground-state phase diagram (see Fig.2 (c)) has been determined accurately by the quantum Monte Carlo method [68]. The inverse temperature

$\beta = 2L$  suffices to successfully achieve the desired data quality with high efficiency. In the following simulation, we fix the  $J_2 = 1$  and tune the  $J_1$  from  $0_+$  to 1. It's worth noting that the ground state is a dimer product state when  $J_1 \rightarrow 0$ , where the  $Z_A^{(n)}/Z^n = 1$  once the dimers are not cut by the entangled edge.

In the SSE frame, the Eq.(1) is equal to

$$\frac{Z_A^{(n)}(J_1')}{Z_A^{(n)}(J_1)} = \left\langle \left( \frac{J_1'}{J_1} \right)^{n_{J_1}} \right\rangle_{Z_A^{(n)}(J_1)} \quad (4)$$

where the  $n_{J_1}$  is the number of  $J_1$  operators in the SSE sampling, no matter which space-time manifold  $Z_A^{(n)}$  is simulated. The details of this equation can be found in the Supplementary Materials (SM).

In the realistic simulation, we need to calculate  $Z_A^{(2)}(J_1')/Z_A^{(2)}(J_1 = 0_+)$  and  $Z(J_1')/Z(J_1 = 0_+)$  respectively. And then obtain the final ratio  $[Z_A^{(2)}/Z^2]_{J_1}$  based on  $[Z_A^{(2)}/Z^2]_{J_1=0_+} = 1$ . Although the parameter is continuously tunable which is same as the non-equilibrium method [22, 53, 57], the incremental path of our method is physical and meaningful. It is a real parameter path of the concerned Hamiltonian. In another word, under similar computational cost, the previous method obtains a point while ours gains a curve of EE data. Even ignoring the low-technical-barrier advantage of our method, the efficiency of our calculation is also much higher in this sense.

TABLE I. Fitting results for the data in Fig.3 (a<sub>1</sub>) with  $S^{(2)}(l) = al + bln l - c$ . Reduced and p-value of  $\chi^2$  (R/P- $\chi^2$ ) are also listed.

$J_1$	$a$	$b$	$c$	R/P- $\chi^2$
1.0	0.089(2)	1.05(4)	1.61(9)	1.00/0.40
0.9	0.085(2)	1.02(3)	1.54(7)	0.54/0.71
0.8	0.079(2)	1.06(5)	1.6(1)	1.55/0.19
0.6	0.072(2)	1.06(5)	2.0(2)	1.93/0.10
0.55	0.078(3)	0.8(1)	1.6(2)	3.16/0.02
0.54	0.08(1)	0.6(1)	1.2(2)	2.49/0.04
$J_c = 0.52337$	0.8(1)	0.15(17)	0.1(5)	2.02/0.1

**Cornerless cutting.**- Firstly, we try to calculate the EE with cornerless cutting as shown in Fig.2 (a). According to the previous works [20, 22, 23], only the entangled edge without dimers gives the correct results consistent with CFT prediction. In the Fig. 3 (a<sub>1</sub>), we shows several curves of EE data with different  $J_1$ . The area law fitting data are shown in Table. I. According to the theoretical prediction [71],  $b = N_G/2 = 1$  in the Néel phase of the AFM  $J_1 - J_2$  Heisenberg model, where  $N_G$  means the number of the Goldstone modes. The Table. I shows consistent results that the  $b \sim 1$  at  $J_1 = 1.0, 0.9, 0.8, 0.6$  and  $b$  becomes smaller while  $J_1$  gets closer to the  $O(3)$  critical point  $J_c$ . The theoretical calculation [72] pointed out that the  $b = 0$  at a Wilson-Fisher  $O(N)$  quantum

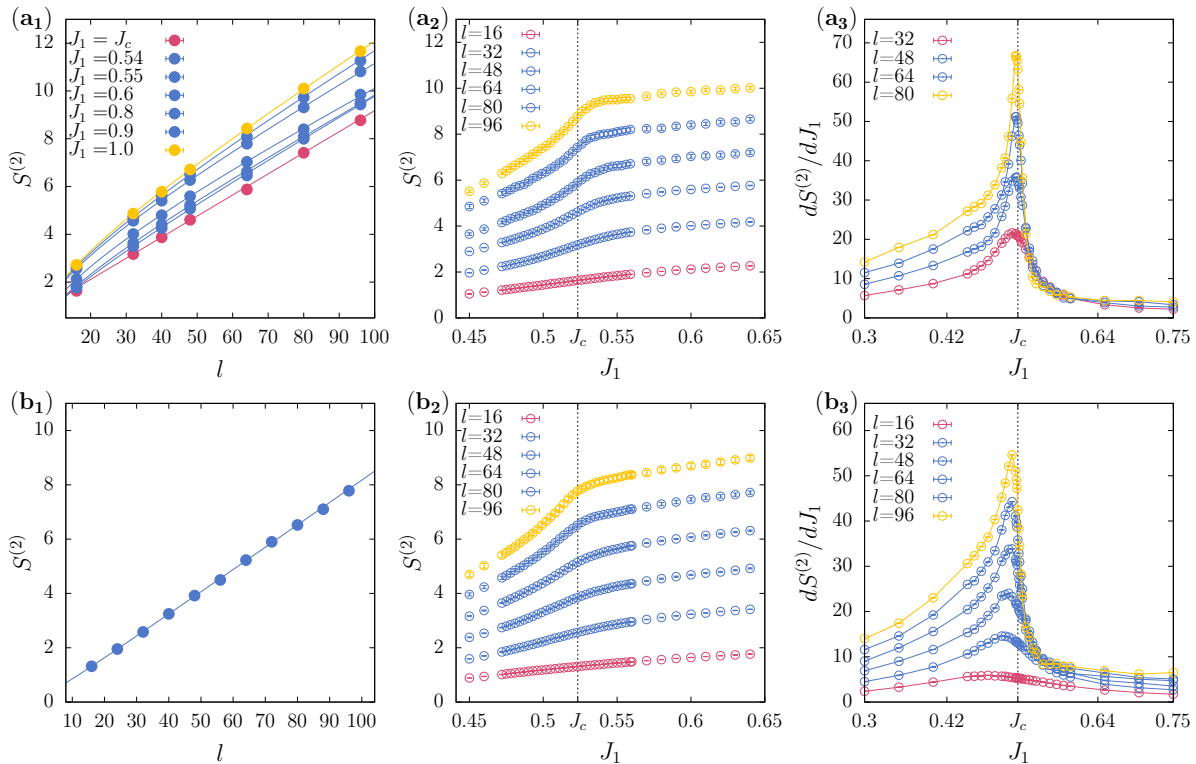


FIG. 3. Second Rényi entanglement entropy  $S^{(2)}$  of the  $J_1 - J_2$  Heisenberg model with the entanglement region  $A$  cornerless [(a<sub>1</sub>),(a<sub>2</sub>) and (a<sub>3</sub>)] or cornered [(b<sub>1</sub>),(b<sub>2</sub>) and (b<sub>3</sub>)]. Cornerless see Fig.2 (a) and cornered see Fig.2 (b). (a<sub>1</sub>)  $S^{(2)}$  versus  $l$  for different couplings  $J_1$ . The fitting results are listed in Table I. (b<sub>1</sub>)  $S^{(2)}$  versus  $l$  at the QCP  $J_1 = J_c = 0.52337$ . The fitting result is  $S^{(2)}(l) = 0.083(1)l - 0.08(1)\ln l + 0.19(2)$  with R/P- $\chi^2$  are 0.85/0.56. [(a<sub>2</sub>) and (b<sub>2</sub>) ]  $S^{(2)}$  versus couplings  $J_1$  for different  $l$  to identify the critical point. [(a<sub>3</sub>) and (b<sub>3</sub>) ] The derivative of  $S^{(2)}$ ,  $dS^{(2)}/dJ_1$ , versus couplings  $J_1$  for different  $l$ . The peaks of  $dS^{(2)}/dJ_1$  appear at the QCP  $J_c$ .

criticality of  $d \geq 2$  systems. Our result at  $J_c$  in the Table also supports this prediction. We note that the recent work [73] found the finite size effect in the spin-1/2 AFM Heisenberg model is strong which obviously affects the fitting of  $b = 1$ , and a good fitting needs some more corrections considering the finite size effect. However, we find the simple fitting is not bad in our results. The reason may be the total system we chose is a rectangle and the region  $A$  is a square, while they chose a square total system and rectangle  $A$ . Other QMC works with similar cutting choice as ours also obtains the  $b \sim 1$  through the non-equilibrium algorithm [22, 57]. Actually, the finite size effect is more serious in a square total system than a rectangle one, which can also be reflected in Fig. 3 (a<sub>3</sub>) and (b<sub>3</sub>). In the figures we found the derivative of EE obviously converges to the critical point faster in a rectangle case than a square one. We will discuss these data more in the following section.

Another advantage of our method is naturally obtaining the EE of different parameter values, as shown in Fig. 3 (a<sub>2</sub>). It makes QMC possible to probe the phase transition via EE in 2D and higher dimensional systems as same as the density matrix renormalization group

(DMRG) usually does in 1D [74–78]. In the Fig. 3 (a<sub>2</sub>), the convexity of the function changes at the critical point, which can also be seen in the derivative of EE more obviously. In the following section, we will introduce a much simpler way to calculate the derivative of EE without incremental process and show the peak of the derivative locates at the phase transition point. It's worth noting that sometimes the original function of EE directly probe the phase transition while sometimes the derivative does. This issue will be carefully discussed in our coming work [79].

*Cornered cutting.-* For the cornered cutting case, the  $b \sim 0.08$  at the 2+1d O(3) quantum criticality is also known according to previous theoretical and numerical works [20, 22, 80–82]. In the Fig. 3 (b<sub>1</sub>), the fitting obtains the consistent result  $b = 0.08(1)$  at  $J_c$ . Similar to the cornerless case, the function EE of  $J_1$  also displays a change of the convexity at the quantum criticality as shown in Fig. 3 (b<sub>2</sub>).

*EE derivative.-* It can be proved in the SM that the derivative of the  $n$ th Rényi EE can be measured in the

form:

$$\frac{dS^{(n)}}{dJ} = \frac{1}{1-n} \left[ -n\beta \left\langle \frac{dH}{dJ} \right\rangle_{Z_A^{(n)}} + n\beta \left\langle \frac{dH}{dJ} \right\rangle_Z \right] \quad (5)$$

where the  $J$  is a general parameter and  $n$  is the Rényi index, the first average is based on the distribution of  $Z_A^{(n)}$  and the second is  $Z$ . Taking the  $J_1 - J_2$  model as an example with fixed  $J_2 = 1$  and  $n = 2$ , set  $J_1$  as the tunable parameter here and note  $H$  is a linear function of  $J_1$ , the Eq.(5) becomes  $dS^{(2)}/dJ_1 = 2\beta \langle H_{J_1}/J_1 \rangle_{Z_A^{(2)}} - 2\beta \langle H_{J_1}/J_1 \rangle_Z$ , where the  $H_{J_1}$  means the  $J_1$  term of the  $H$ . In the SSE frame, it is similar as measuring energy value, which is very simple. The details can be found in the SM.

This conclusion inspires us that we do not need calculating dense data of EE to obtain the derivative. Instead, simulate the average,  $2\beta \langle H_{J_1}/J_1 \rangle_{Z_A^{(2)}} - 2\beta \langle H_{J_1}/J_1 \rangle_Z$ , at the  $J_1$  we concern directly is enough. We found a similar spirit has been used in calculating the derivative of the Rényi negativity versus the inverse temperature [83]. Through this method, we calculate the derivative of EE curves in the Fig. 3 (a<sub>2</sub>) and Fig. 3 (b<sub>2</sub>). As shown in Fig. 3 (a<sub>3</sub>) and Fig. 3 (b<sub>3</sub>), the peaks of the EE derivative really locate at the phase transition point.

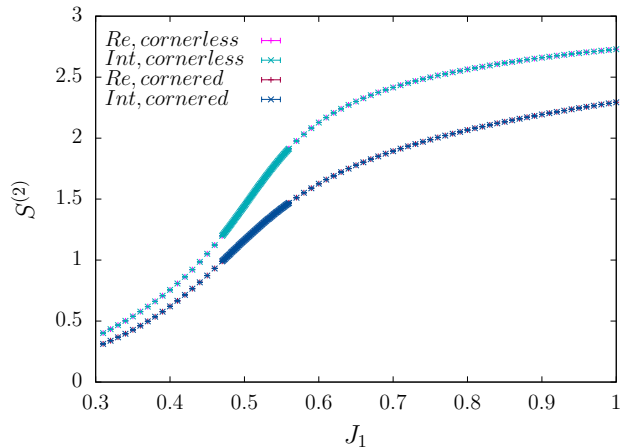


FIG. 4. Second Rényi entanglement entropy  $S^{(2)}$  of the  $J_1 - J_2$  Heisenberg model as a function of the coupling  $J_1$  are calculated by Reweight method (Re) and integral method (Int) either in cornerless or cornered entanglement region  $A$  with  $l = 16$ . With or without corners, the results are consistent within errorbar for two methods.

In fact, this measurement of the EE derivative also points out another way for calculating the EE value through an integral

$$S^{(n)}(J') = \int_{J_0}^{J'} \frac{dS^{(n)}}{dJ} dJ + S^{(n)}(J_0) \quad (6)$$

where the  $dS^{(n)}/dJ$  can be gained through Eq. (5) and the EE  $S^{(n)}(J_0)$  at the reference point should be known,

such as a product state. We demonstrate the equivalence of the two ways (Eq. (4) and Eq. (6)) by taking the  $J_1 - J_2$  model as an example, as shown in the Fig. 4, either in cornerless or cornered case.

We note Jarzynski's equality [84] can also be used in our methods, similar to the previous non-equilibrium algorithms [53, 57]. But we found that there is almost no acceleration effect for the non-equilibrium version compared with the equilibrium QMC, the details in which will be discussed in our coming work [85].

**Conclusion.** - Overall, we develop a practical and unbiased scheme with low-technical barrier to extract the high-precision EE and its derivative from QMC simulation. The space-time manifold needn't be changed during the simulation and the measurement is an easy diagonal observable. All the intermediate-process measurement-quantities are meaningful and physical, which is un wasteful and useful. It makes QMC possible to probe the novel phases and phase transition by scanning EE in a large parameter region in 2D and higher dimensional systems as same as the DMRG usually does in 1D.

We display a simulating-path from a dimer product state to a Néel phase by taking the  $J_1 - J_2$  AFM Heisenberg model as an example. A diverging peak of EE derivative arises at the phase transition point. The universal coefficient of the sub-leading term of the EE has been successfully extracted in high precision, either at O(3) criticality or continuous-symmetry-breaking phase. Our method is not only limited to boson QMC, but can also be used to other QMC approaches, such as the fermion QMC [86], for highly entangled quantum matter.

**Acknowledgement** We thank the helpful discussions with Jiarui Zhao, Dong-Xu Liu, Yin Tang, Zehui Deng, Bin-Bin Chen, Yuan Da Liao, and Wei Zhu. ZY acknowledges the collaborations with Yan-Cheng Wang, Z. Y. Meng and Meng Cheng in other related works. The work is supported by the start-up funding of Westlake University. The authors thank the high-performance computing center of Westlake University and the Beijing PARATERA Tech Co.,Ltd. for providing HPC resources.

### Details about the derivative of entanglement entropy

The Rényi entanglement entropy (EE) is defined as

$$S^{(n)} = \frac{1}{1-n} \ln \frac{Z_A^{(n)}}{Z^n} \quad (7)$$

where

$$Z = \text{Tr} e^{-\beta H} \quad (8)$$

and

$$Z_A^{(n)} = \text{Tr}[(\text{Tr}_B e^{-\beta H})^n] \quad (9)$$

Thus the EE derivative of  $J$  is

$$\frac{dS^{(n)}}{dJ} = \frac{1}{1-n} \left[ \frac{dZ_A^{(n)}/dJ}{Z_A^{(n)}} - n \frac{dZ/dJ}{Z} \right] \quad (10)$$

According to the Eq.(8), we have

$$\frac{dZ}{dJ} = \text{Tr}[-\beta \frac{dH}{dJ} e^{-\beta H}] \quad (11)$$

Thus

$$\frac{dZ/dJ}{Z} = -\beta \left\langle \frac{dH}{dJ} \right\rangle_Z \quad (12)$$

Similarly, because partial trace is a linear operator which is commutative with the derivative operator, we have

$$\begin{aligned} \frac{dZ_A^{(n)}/dJ}{Z_A^{(n)}} &= \frac{\text{Tr}[-n\beta(\text{Tr}_B e^{-\beta H})^{n-1}(\text{Tr}_B e^{-\beta H} \frac{dH}{dJ})]}{\text{Tr}[(\text{Tr}_B e^{-\beta H})^n]} \\ &= -n\beta \left\langle \frac{dH}{dJ} \right\rangle_{Z_A^{(n)}} \end{aligned} \quad (13)$$

Therefore, the EE derivative can be rewritten as

$$\frac{dS^{(n)}}{dJ} = \frac{1}{1-n} \left[ -n\beta \left\langle \frac{dH}{dJ} \right\rangle_{Z_A^{(n)}} + n\beta \left\langle \frac{dH}{dJ} \right\rangle_Z \right] \quad (14)$$

The equations above is very general and doesn't depend on detailed QMC methods. Then let us see how to calculate them in SSE simulation. For convenience, we fix the Rényi index  $n = 2$  and choose  $J_1 - J_2$  model of the main text as the example for explaining technical details. The Hamiltonian is

$$H = J_1 \sum_{\langle ij \rangle} S_i S_j + J_2 \sum_{\langle ij \rangle} S_i S_j \quad (15)$$

In the followings, we fix the  $J_2 = 1$  and leave the  $J_1$  as the tunable parameter. Note the Hamiltonian is a linear function of  $J_1$ , that means  $dH/dJ_1 = H_{J_1}/J_1$  in which

$H_{J_1}$  is partial Hamiltonian  $H(J_2 = 0, J_1)$ . Then the EE derivative is simplified as

$$\frac{dS^{(2)}}{dJ_1} = \left[ 2\beta \left\langle \frac{H_{J_1}}{J_1} \right\rangle_{Z_A^{(2)}} - 2\beta \left\langle \frac{H_{J_1}}{J_1} \right\rangle_Z \right] \quad (16)$$

In the SSE frame, it is easy to obtain  $\langle H \rangle = \langle -n_{op}/\beta \rangle$  [?], where  $n_{op}$  is the number of the concerned Hamiltonian operators. Thus the Eq. (16) can be further simplified to

$$\frac{dS^{(2)}}{dJ_1} = \left[ - \left\langle \frac{n_{J_1}}{J_1} \right\rangle_{Z_A^{(2)}} + 2 \left\langle \frac{n_{J_1}}{J_1} \right\rangle_Z \right] \quad (17)$$

where  $n_{J_1}$  means the number of  $J_1$  operators including both diagonal and off-diagonal ones. It's worth noting that there is no "2" anymore in the  $\langle \dots \rangle_{Z_A^{(2)}}$  term, because  $n_{J_1}$  here contains two replicas' operators which has already been doubled actually.

So far, we have explained how to define the EE derivative in general QMC methods and measure it in detailed SSE algorithm. As shown in the main text, the integral of the EE derivative is highly consistent with the EE original function, which provides another way to obtain EE. The EE derivative also successfully help us to probe quantum phase transition through either conered or cornerless cutting.

### The weight ratio in SSE

In the SSE, the partition function can be expanded as [39? ],

$$\begin{aligned} Z &= \sum_{\{\alpha_i\}} \frac{\beta^n (M-n)!}{M!} \langle \alpha_1 | H_{12} | \alpha_2 \rangle \times \\ &\quad \langle \alpha_2 | H_{23} | \alpha_3 \rangle \dots \langle \alpha_M | H_{M1} | \alpha_1 \rangle \\ &= \sum_{\{\alpha_i\}} W(\{\alpha_i\}) \end{aligned} \quad (18)$$

where  $n$  is the number of non-identity operators and  $M$  is the total number of all the operators.  $H_{ij}$  means the operator connects two closest states  $\alpha_i$  and  $\alpha_j$ .

In the reweighting process, for example, if we only tune the parameter  $J_1$ , the weight ratio under a fixed  $\{\alpha_i\}$  will becomes

$$\frac{W(J_1')}{W(J_1)} = \left( \frac{J_1'}{J_1} \right)^{n_{J_1}} \quad (19)$$

where the  $n_{J_1}$  is the number of  $J_1$  operators. The Eq. (19) comes from the Eq. (18), because only the elements  $\langle \alpha_i | H_{ij} | \alpha_j \rangle$  in which the  $H_{ij}$  is  $J_1$  term will affect the ratio.

Similarly, we can get the weight ratio in a general partition function  $Z_A^{(n)}$ . In fact, its result is also the Eq. (19).

### Details about calculating $R_A^{(n)}$

As mentioned in the main text, in principle, if  $Z_A^{(n)}(J_{1(i+1)})/Z_A^{(n)}(J_{1(i)})$  tends to 1, the calculation results will be more accurate according to the importance sampling, but it requires more segmentation. Moderately, we can choose a value which is not too small or large, near 1. In this paper, we set the smallest value of  $Z_A^{(n)}(J_{1(i+1)})/Z_A^{(n)}(J_{1(i)}) \sim 0.2$ . For the model we studied, the  $n_{J_1}$  will increase with  $J_1$  and  $\sim \beta L^2$  at  $J_1 = J_2 = 1$ . Based on this, we can estimate the value of  $J_{ratio} = J_{1(i+1)}/J_{1(i)}$  as  $J_{ratio} \sim e^{\ln[0.2]/(\beta L^2)}$ .

The next question is how to determine the value of the  $N$  in

$$\begin{aligned} \frac{Z_A^{(n)}(J'_1)}{Z_A^{(n)}(J_1)} &= \prod_{i=0}^{N-1} \frac{Z_A^{(n)}(J_{1(i+1)})}{Z_A^{(n)}(J_{1(i)})} = \prod_{i=0}^{N-1} \left\langle \frac{W(J_{1(i+1)})}{W(J_{1(i)})} \right\rangle_{Z_A^{(n)}} \\ &= \prod_{i=0}^{N-1} \left\langle \left( \frac{J_{1(i+1)}}{J_{1(i)}} \right)^{n_{J_1}} \right\rangle_{Z_A^{(n)}} \end{aligned} \quad (20)$$

In principle,  $J_{1(0)}$  should be zero since we choose the product state  $|A\rangle \otimes |B\rangle$  as reference point to calculate Rényi entropy at  $J_{1(N)}$ . However we cannot and do not need to reach  $J_{1(0)} = 0$  in the actual simulation. We only need to ensure that  $Z_A^{(n)}(J_{1(1)})/Z_A^{(n)}(J_{1(0)}) = 1$  in the sampling time. To do this, we divide  $N$  into  $N = N_1 + N_2$ . The first step is to reach  $J_{1(N)}(J_{ratio})^{N_1} = 0.001$ , i.e.  $N_1 = e^{\ln[0.001/J_{1(N)}]/\ln[J_{ratio}]}$ . The second step is to reach  $J_{1(N)}(J_{ratio})^{N_1+N_2} = J_{1(0)} = 0_+$ , at which  $Z_A^{(n)}(J_{1(1)})/Z_A^{(n)}(J_{1(0)}) = 1$  in the sampling and the  $N_2$  is determined by the computer.

---

\* zhengyan@westlake.edu.cn

- [1] L. Amico, R. Fazio, A. Osterloh, and V. Vedral, Entanglement in many-body systems, *Rev. Mod. Phys.* **80**, 517 (2008).
- [2] N. Laflorencie, Quantum entanglement in condensed matter systems, *Physics Reports* **646**, 1 (2016), quantum entanglement in condensed matter systems.
- [3] G. Vidal, J. I. Latorre, E. Rico, and A. Kitaev, Entanglement in quantum critical phenomena, *Phys. Rev. Lett.* **90**, 227902 (2003).
- [4] V. E. Korepin, Universality of entropy scaling in one-dimensional gapless models, *Phys. Rev. Lett.* **92**, 096402 (2004).
- [5] A. Kitaev and J. Preskill, Topological entanglement entropy, *Phys. Rev. Lett.* **96**, 110404 (2006).
- [6] M. Levin and X.-G. Wen, Detecting topological order in a ground state wave function, *Phys. Rev. Lett.* **96**, 110405 (2006).
- [7] P. Calabrese and A. Lefevre, Entanglement spectrum in one-dimensional systems, *Phys. Rev. A* **78**, 032329 (2008).
- [8] E. Fradkin and J. E. Moore, Entanglement entropy of 2d conformal quantum critical points: Hearing the shape of a quantum drum, *Phys. Rev. Lett.* **97**, 050404 (2006).
- [9] Z. Nussinov and G. Ortiz, Sufficient symmetry conditions for Topological Quantum Order, *Proc. Nat. Acad. Sci.* **106**, 16944 (2009).
- [10] Z. Nussinov and G. Ortiz, A symmetry principle for topological quantum order, *Annals Phys.* **324**, 977 (2009).
- [11] H. Casini and M. Huerta, Universal terms for the entanglement entropy in 2+1 dimensions, *Nuclear Physics B* **764**, 183 (2007).
- [12] W. Ji and X.-G. Wen, Noninvertible anomalies and mapping-class-group transformation of anomalous partition functions, *Phys. Rev. Research* **1**, 033054 (2019).
- [13] W. Ji and X.-G. Wen, Categorical symmetry and noninvertible anomaly in symmetry-breaking and topological phase transitions, *Phys. Rev. Research* **2**, 033417 (2020).
- [14] L. Kong, T. Lan, X.-G. Wen, Z.-H. Zhang, and H. Zheng, Algebraic higher symmetry and categorical symmetry: A holographic and entanglement view of symmetry, *Phys. Rev. Research* **2**, 043086 (2020).
- [15] X.-C. Wu, W. Ji, and C. Xu, Categorical symmetries at criticality, *Journal of Statistical Mechanics: Theory and Experiment* **2021**, 073101 (2021).
- [16] W. Ding, N. E. Bonesteel, and K. Yang, Block entanglement entropy of ground states with long-range magnetic order, *Physical Review A* **77**, 052109 (2008).
- [17] Q.-C. Tang and W. Zhu, Critical scaling behaviors of entanglement spectra, *Chinese Physics Letters* **37**, 010301 (2020).
- [18] J. Zhao, Z. Yan, M. Cheng, and Z. Y. Meng, Higher-form symmetry breaking at ising transitions, *Phys. Rev. Research* **3**, 033024 (2021).
- [19] X.-C. Wu, C.-M. Jian, and C. Xu, Universal Features of Higher-Form Symmetries at Phase Transitions, *SciPost Phys.* **11**, 33 (2021).
- [20] J. Zhao, Y.-C. Wang, Z. Yan, M. Cheng, and Z. Y. Meng, Scaling of entanglement entropy at deconfined quantum criticality, *Physical Review Letters* **128**, 010601 (2022).
- [21] B.-B. Chen, H.-H. Tu, Z. Y. Meng, and M. Cheng, Topological disorder parameter: A many-body invariant to characterize gapped quantum phases, *Phys. Rev. B* **106**, 094415 (2022).
- [22] J. Zhao, B.-B. Chen, Y.-C. Wang, Z. Yan, M. Cheng, and Z. Y. Meng, Measuring rényi entanglement entropy with high efficiency and precision in quantum monte carlo simulations, *npj Quantum Materials* **7**, 69 (2022).
- [23] Y.-C. Wang, N. Ma, M. Cheng, and Z. Y. Meng, Scaling of the disorder operator at deconfined quantum criticality, *SciPost Physics* **13**, 123 (2022).
- [24] Y.-C. Wang, M. Cheng, and Z. Y. Meng, Scaling of the disorder operator at  $(2+1)d$   $u(1)$  quantum criticality, *Phys. Rev. B* **104**, L081109 (2021).
- [25] W. Jiang, B.-B. Chen, Z. H. Liu, J. Rong, F. F. Asaad, M. Cheng, K. Sun, and Z. Y. Meng, Many versus one: The disorder operator and entanglement entropy in fermionic quantum matter, *SciPost Phys.* **15**, 082 (2023).
- [26] Z. Yan and Z. Y. Meng, Unlocking the general relationship between energy and entanglement spectra via the wormhole effect, *Nature Communications* **14**, 2360 (2023).
- [27] T. Senthil, A. Vishwanath, L. Balents, S. Sachdev, and M. P. Fisher, Deconfined quantum critical points, *Science* **303**, 1490 (2004).

- [28] T. Senthil, L. Balents, S. Sachdev, A. Vishwanath, and M. P. Fisher, Quantum criticality beyond the landau-ginzburg-wilson paradigm, *Physical Review B* **70**, 144407 (2004).
- [29] H. Shao, W. Guo, and A. W. Sandvik, Quantum criticality with two length scales, *Science* **352**, 213 (2016).
- [30] A. W. Sandvik, Evidence for deconfined quantum criticality in a two-dimensional heisenberg model with four-spin interactions, *Physical review letters* **98**, 227202 (2007).
- [31] J. Lou, A. W. Sandvik, and N. Kawashima, Antiferromagnetic to valence-bond-solid transitions in two-dimensional  $su(n)$  heisenberg models with multispin interactions, *Physical Review B* **80**, 180414 (2009).
- [32] Z. Deng, L. Liu, W. Guo, and H.-q. Lin, Diagnosing  $so(5)$  symmetry and first-order transition in the  $j - q_3$  model via entanglement entropy, arXiv preprint arXiv:2401.12838 (2024).
- [33] J. D’Emidio and A. W. Sandvik, Entanglement entropy and deconfined criticality: emergent  $so(5)$  symmetry and proper lattice bipartition, arXiv preprint arXiv:2401.14396 (2024).
- [34] M. Song, J. Zhao, L. Janssen, M. M. Scherer, and Z. Y. Meng, Deconfined quantum criticality lost, arXiv preprint arXiv:2307.02547 (2023).
- [35] M. Song, J. Zhao, Z. Y. Meng, C. Xu, and M. Cheng, Extracting subleading corrections in entanglement entropy at quantum phase transitions, arXiv preprint arXiv:2312.13498 (2023).
- [36] G. Torlai and R. G. Melko, Corner entanglement of a resonating valence bond wavefunction (2024), arXiv:2402.17211 [cond-mat.str-el].
- [37] H. Casini and M. Huerta, Universal terms for the entanglement entropy in  $2+1$  dimensions, *Nuclear Physics B* **764**, 183 (2007).
- [38] H. Casini and M. Huerta, Positivity, entanglement entropy, and minimal surfaces, *Journal of High Energy Physics* **2012**, 1 (2012).
- [39] A. W. Sandvik, Stochastic series expansion method with operator-loop update, *Phys. Rev. B* **59**, R14157 (1999).
- [40] A. W. Sandvik, Computational Studies of Quantum Spin Systems, *AIP Conference Proceedings* **1297**, 135 (2010).
- [41] A. W. Sandvik, Stochastic series expansion methods, arXiv:1909.10591.
- [42] O. F. Syljuåsen and A. W. Sandvik, Quantum monte carlo with directed loops, *Phys. Rev. E* **66**, 046701 (2002).
- [43] Z. Yan, Global scheme of sweeping cluster algorithm to sample among topological sectors, *Phys. Rev. B* **105**, 184432 (2022).
- [44] M. Suzuki, S. Miyashita, and A. Kuroda, Monte carlo simulation of quantum spin systems. i, *Progress of Theoretical Physics* **58**, 1377 (1977).
- [45] J. E. Hirsch, R. L. Sugar, D. J. Scalapino, and R. Blankenbecler, Monte carlo simulations of one-dimensional fermion systems, *Phys. Rev. B* **26**, 5033 (1982).
- [46] M. Suzuki, Relationship between  $d$ -dimensional quantum spin systems and  $(d+1)$ -dimensional ising systems: Equivalence, critical exponents and systematic approximants of the partition function and spin correlations, *Progress of theoretical physics* **56**, 1454 (1976).
- [47] H. W. J. Blöte and Y. Deng, Cluster monte carlo simulation of the transverse ising model, *Phys. Rev. E* **66**, 066110 (2002).
- [48] C.-J. Huang, L. Liu, Y. Jiang, and Y. Deng, Worm-algorithm-type simulation of the quantum transverse-field ising model, *Physical Review B* **102**, 094101 (2020).
- [49] Z. Fan, C. Zhang, and Y. Deng, Clock factorized quantum monte carlo method for long-range interacting systems (2023), arXiv:2305.14082 [physics.comp-ph].
- [50] M. B. Hastings, I. González, A. B. Kallin, and R. G. Melko, Measuring renyi entanglement entropy in quantum monte carlo simulations, *Phys. Rev. Lett.* **104**, 157201 (2010).
- [51] S. Humeniuk and T. Roscilde, Quantum monte carlo calculation of entanglement rényi entropies for generic quantum systems, *Phys. Rev. B* **86**, 235116 (2012).
- [52] T. Grover, Entanglement of interacting fermions in quantum monte carlo calculations, *Phys. Rev. Lett.* **111**, 130402 (2013).
- [53] V. Alba, Out-of-equilibrium protocol for rényi entropies via the jarzynski equality, *Physical Review E* **95**, 062132 (2017).
- [54] D. J. Luitz, X. Plat, N. Laflorencie, and F. Alet, Improving entanglement and thermodynamic rényi entropy measurements in quantum monte carlo, *Phys. Rev. B* **90**, 125105 (2014).
- [55] L. Wang and M. Troyer, Rényi entanglement entropy of interacting fermions calculated using the continuous-time quantum monte carlo method, *Phys. Rev. Lett.* **113**, 110401 (2014).
- [56] C. M. Herdman, S. Inglis, P.-N. Roy, R. G. Melko, and A. Del Maestro, Path-integral monte carlo method for rényi entanglement entropies, *Phys. Rev. E* **90**, 013308 (2014).
- [57] J. D’Emidio, Entanglement entropy from nonequilibrium work, *Phys. Rev. Lett.* **124**, 110602 (2020).
- [58] M. Song, T.-T. Wang, and Z. Y. Meng, Resummation-based quantum monte carlo for entanglement entropy computation (2023), arXiv:2310.01490 [cond-mat.str-el].
- [59] X. Zhou, Z. Y. Meng, Y. Qi, and Y. Da Liao, Incremental swap operator for entanglement entropy: Application for exponential observables in quantum monte carlo simulation, *Phys. Rev. B* **109**, 165106 (2024).
- [60] C. Li, R.-Z. Huang, Y.-M. Ding, Z. Y. Meng, Y.-C. Wang, and Z. Yan, Relevant long-range interaction of the entanglement hamiltonian emerges from a short-range gapped system, *Phys. Rev. B* **109**, 195169 (2024).
- [61] S. Wu, X. Ran, B. Yin, Q.-F. Li, B.-B. Mao, Y.-C. Wang, and Z. Yan, Classical model emerges in quantum entanglement: Quantum monte carlo study for an ising-heisenberg bilayer, *Phys. Rev. B* **107**, 155121 (2023).
- [62] M. Song, J. Zhao, Z. Yan, and Z. Y. Meng, Different temperature dependence for the edge and bulk of the entanglement hamiltonian, *Phys. Rev. B* **108**, 075114 (2023).
- [63] Z. Liu, R.-Z. Huang, Z. Yan, and D.-X. Yao, Demonstrating the wormhole mechanism of the entanglement spectrum via a perturbed boundary, *Phys. Rev. B* **109**, 094416 (2024).
- [64] B.-B. Mao, Y.-M. Ding, and Z. Yan, Sampling reduced density matrix to extract fine levels of entanglement spectrum, arXiv preprint arXiv:2310.16709 (2023).
- [65] Y.-M. Ding, J.-S. Sun, N. Ma, G. Pan, C. Cheng, and Z. Yan, Reweight-annealing method for calculating the value of partition function via quantum monte carlo (2024), arXiv:2403.08642 [cond-mat.stat-mech].
- [66] Z. Dai and X. Y. Xu, Residual entropy from tem-



- perature incremental monte carlo method (2024), arXiv:2402.17827 [cond-mat.stat-mech].
- [67] R. M. Neal, Annealed importance sampling, *Statistics and computing* **11**, 125 (2001).
- [68] M. Matsumoto, C. Yasuda, S. Todo, and H. Takayama, Ground-state phase diagram of quantum heisenberg antiferromagnets on the anisotropic dimerized square lattice, *Phys. Rev. B* **65**, 014407 (2001).
- [69] C. Ding, L. Zhang, and W. Guo, Engineering surface critical behavior of  $(2+1)$ -dimensional  $o(3)$  quantum critical points, *Physical Review Letters* **120**, 235701 (2018).
- [70] Z. Yan, Y. Wu, C. Liu, O. F. Syljuåsen, J. Lou, and Y. Chen, Sweeping cluster algorithm for quantum spin systems with strong geometric restrictions, *Physical Review B* **99**, 165135 (2019).
- [71] M. A. Metlitski and T. Grover, Entanglement entropy of systems with spontaneously broken continuous symmetry, arXiv preprint arXiv:1112.5166 (2011).
- [72] M. A. Metlitski, C. A. Fuertes, and S. Sachdev, Entanglement entropy in the  $o(n)$  model, *Physical Review B* **80**, 115122 (2009).
- [73] Z. Deng, L. Liu, W. Guo, and H. Lin, Improved scaling of the entanglement entropy of quantum antiferromagnetic heisenberg systems, *Physical Review B* **108**, 125144 (2023).
- [74] J. I. Latorre, E. Rico, and G. Vidal, Ground state entanglement in quantum spin chains (2004), arXiv:quant-ph/0304098 [quant-ph].
- [75] O. Legeza and J. Sólyom, Two-site entropy and quantum phase transitions in low-dimensional models, *Phys. Rev. Lett.* **96**, 116401 (2006).
- [76] W.-L. Chan and S.-J. Gu, Entanglement and quantum phase transition in the asymmetric hubbard chain: Density-matrix renormalization group calculations, *Journal of Physics Condensed Matter* **20** (2008).
- [77] J. Ren, X. Xu, L. Gu, and J. Li, Quantum information analysis of quantum phase transitions in a one-dimensional  $V_1$ - $V_2$  hard-core-boson model, *Phys. Rev. A* **86**, 064301 (2012).
- [78] P. Laurell, A. Scheie, C. J. Mukherjee, M. M. Koza, M. Enderle, Z. Tylczynski, S. Okamoto, R. Coldea, D. A. Tennant, and G. Alvarez, Quantifying and controlling entanglement in the quantum magnet  $cs_2cocl_4$ , *Phys. Rev. Lett.* **127**, 037201 (2021).
- [79] Zhe Wang, Zheng Yan, et al. In preparation.
- [80] S. Inglis and R. G. Melko, Wang-landau method for calculating rényi entropies in finite-temperature quantum monte carlo simulations, *Phys. Rev. E* **87**, 013306 (2013).
- [81] A. B. Kallin, E. M. Stoudenmire, P. Fendley, R. R. P. Singh, and R. G. Melko, Corner contribution to the entanglement entropy of an  $O(3)$  quantum critical point in  $2 + 1$  dimensions, *J. Stat. Mech.* **2014**, 06009 (2014), arXiv:1401.3504.
- [82] J. Helmes and S. Wessel, Entanglement entropy scaling in the bilayer heisenberg spin system, *Phys. Rev. B* **89**, 245120 (2014).
- [83] K.-H. Wu, T.-C. Lu, C.-M. Chung, Y.-J. Kao, and T. Grover, Entanglement renyi negativity across a finite temperature transition: a monte carlo study, *Physical Review Letters* **125**, 140603 (2020).
- [84] C. Jarzynski, Nonequilibrium equality for free energy differences, *Phys. Rev. Lett.* **78**, 2690 (1997).
- [85] Zhe Wang, Zhiyan Wang, Yi-Ming Ding, Zheng Yan, et al. In preparation.
- [86] Weilun Jiang, Zheng Yan, et al. In preparation.